ELSEVIER

Journal of Alloys and Compounds 261 (1997) 225–230

Journal of ALLOYS AND COMPOUNDS

SANS measurements of deuterium-dislocation trapping in deformed single crystal Pd

Brent J. Heuser[a,*], John S. King[b]

[a]*University of Illinois, Department of Nuclear Engineering, Urbana, IL 61801 USA*
[b]*University of Michigan, Department of Nuclear Engineering, Ann Arbor, MI 48109 USA*

Received 8 January 1997; received in revised form 18 March 1997

Abstract

Small-angle neutron scattering (SANS) measurements have been made on deformed, single crystal Pd at room temperature. Low concentrations of deuterium were introduced to observe dislocation-deuteron interactions. Two different deformation procedures (cold working by rolling and hydride cycling) were used in an attempt to compare dislocations with different substructures. The data appear to fall naturally into an intermediate Q and a low Q region. The intermediate Q region is well described by a $1/Q$ model, which yields effective trapping radius, R_o, and trapping efficiency, $\overline{\rho_D}/\rho_d$ (the number of deuterons per Å of dislocation line). The trapping radii for both sample types are approximately 11 Å but the efficiencies differ by a factor of 2 or more. The conclusion is that in both cases the majority of trapped deuterons lie within a few Burgers vectors of the dislocation cores, but the trapping efficiency is significantly larger for the relatively uniform hydride cycled substructure than for the cold worked substructure. This we attribute to stress compensation from neighbouring dislocations in a cell-wall environment characteristic of the cold worked substructure. In the lowest Q region, the cross section for the cycled samples diverges from that of the cold worked sample, indicating a long rang trapping in the stress field of the former which is absent in the latter. In both Q regions, therefore, trapping is enhanced for the cycled dislocation substructure.

Keywords: Deuterium; Dislocation; Palladium; SANS; Trapping

1. Introduction

Palladium has served as a test-bed material for the study of hydrogen–metal systems for 25 years. This is primarily due to the ability of Pd to absorb hydrogen readily from the gas phase at room temperature and to the α–α' transition resembling a gas-liquid transition of a real gas [1]. The thermodynamics of hydrogen and deuterium in solid solution [2,3], and of the α–α' phase transition [4,5] have been thoroughly investigated. In addition, the diffusivities of hydrogen and deuterium in Pd [6], and to a lesser extent of tritium [7], have been characterized under a wide variety of conditions. In the majority of these experiments, hydrogen solubility or permeability was measured during charging from the gas phase or by using electrochemical methods.

The effect of defect trapping on solid solution thermodynamics and diffusivity using the same experimental techniques have been examined in detail as well [7–9]. And although hydrogen interactions with grain boundary defects have been studied [8,10], the most common trapping defect considered has been the dislocation. The creation of dislocation defects in Pd was found to enhance the solubility of hydrogen in solid solution [8,9]. Significant dislocation densities also resulted in a decrease of hydrogen diffusivity. In fact, a dependence of the apparent diffusion coefficient on hydrogen concentration has been observed, with the measured value approaching the defect-free coefficient as the dislocation traps saturate [8].

More recently, small-angle neutron scattering (SANS) has been used to characterize the dislocation-deuterium trapping interaction in Pd [8,11]. In SANS, the measured coherent scattering cross section is determined only by the local geometry and concentration of trapped deuterium. The technique offers the possibility of probing directly the trapping interaction on a microscopic scale. In particular, the trapped concentration per unit dislocation length and the trapping radius, R_o, can be inferred. Using a simple model to analyze solubility data, Tyson has reported an "extended core" trapping radius of 28 Å for deformed Pd

*Corresponding author.

0925-8388/97/$17.00
PII S0925-8388(97)00211-9

Table 1
Fitting parameters from measured cross sections

Sample	Enhancement Ratio	ρ_D [$\times 10^{20}$ l cm^{-3}]	ρ_d [$\times 10^{11}$ l cm^{-2}]	R_ρ [Å]	L_ρ [Å]	ρ_D/ρ_d [deuterons/Å]
NIST Data (This work)						
SC(α/α′/α)12	1.29	1.01±0.05	2.4±0.2	11	58±1	4.2±0.4
SC(α/α′/α)14	1.30	1.13±0.06	2.2±0.2	11	60±1	5.1±0.5
SC(cw)15	1.20	0.66±0.03	3.2±0.4	11	49±4	2.1±0.2
Saclay Data ([11])						
SC(α/α′/α)	1.37	1.37±0.04	6.8±0.4	7	93±12	2.0±0.2
SC(cw)	1.27	0.96±0.03	6.6±0.4	4	41±5	1.5±0.4

[12], and a comparison with that result will be discussed later.

Experiments similar to the present work have been reported previously by us, and the differences in parameters extracted therefrom give qualitative support to this report [11]. However, these parameters are sensitive to experimental errors and to model fitting. The present results are significantly better in both respects, and lead to a clearer physical picture. In particular, the new data reveal a dependence on dislocation morphology in the trapping interaction which was only vaguely suggested earlier. A summary of the earlier results are included in Table 1 and a comparison of results evaluated below.

2. Experimental

Three deformed samples and one reference sample were prepared from a 99.999% pure single crystal Pd ingot grown by Metal Crystals and Oxides of Cambridge, England. The ingot was grown by the Czochralski method, was of cylindrical geometry with a [110] axis, 10 cm in length and 1.0 cm in diameter. Wafers were cut from the as-grown ingot using a low speed diamond saw, then mechanically polished before and after the deformation step to remove surface irregularities introduced during cutting and deformation. All samples consisted of two wafers stacked together, to increase the surface–to–volume ratio and thereby facilitate deuterium loading. Each wafer was approximately 1 cm diameter, 0.16 cm thick and weighed 1.5 grams (for a total sample mass of 3 grams).

Two samples, SC(α/α′/α)12 and SC(α/α′/α)14, were deformed by hydride cycling. In this procedure, the samples were exposed to pure hydrogen gas in a vacuum manifold at room temperature until the entire volume was converted to the α′ phase. The procedure was completed by allowing the α′→α reversion to take place. Although both the solid solution and hydride phases of Pd are face-centred cubic, a 10% volume expansion accompanies the absorption of hydrogen into the $PdH_{0.6}$ disordered α′ structure [13]. To accommodate this miss-match, dislocations are created, more or less uniformly, as the incoherent phase boundary proceeds through the sample volume. Transition electron microscopy (TEM) analysis has confirmed the homogenous arrangement of dislocations in hydride cycled Pd [14–16].

A third sample, SC(cw)15, was cold worked by rolling in two orthogonal directions at room temperature using 5 inch diameter, low speed hardened steel rollers. This sample was rolled to 70% thickness reduction in seven passes. The direction of thickness reduction corresponded to the original [110] cylinder axis. Dislocations created in Pd during this type of deformation form very heterogeneous, or cellular arrangements, where the majority of dislocations are contained in cell walls that separate regions of low dislocation density. The tendency to form cellular substructures is common in high stacking fault metals driven into the work hardening regime of deformation. Cellular dislocation substructures in cold rolled Pd have been observed by TEM [14].

Samples were loaded with deuterium ex situ in a high vacuum manifold at room temperature just prior to SANS investigation. All four samples were loaded with 5500 to 5600 atomic parts per million (appm) bulk deuterium. Although Pd is still within the solid solution a phase at these bulk levels, it should be noted that the overall concentration will be enhanced in the deformed samples because of defect trapping. Measured enhancement ratios are given in Table 1 and are defined as the ratio of overall deuterium concentration to bulk concentration as given by Sievert's law. Generally, 12 to 15 hours of exposure to D_2 gas were required to reach 5500 appm bulk deuterium. More complete details of the deuterium loading procedure have been given previously [11]. After loading, each sample was quickly transferred to a special environmental gas cell, which was then evacuated, back-filled with the equilibrium D_2 gas pressure (approximately 16 torr), and sealed. The temperature in the guide hall was monitored throughout the experiment and was consistently within one degree of 22°C.

The SANS measurements were performed at the NIST-CNRF using the 30 m NSF instrument [17]. The gas cell was rigidly mounted in the standard spectrometer sample box which was evacuated and back-filled with He. The instrument was configured to probe a Q range from $0.012 \leq Q \leq 0.143$ Å^{-1} using the following settings: source–to–sample distance of 537 cm (seven guides in place), sample–to–detector distance of 335 cm, 5.08 cm

diameter beam stop, 5 cm source aperture, a 10 cm detector offset (to increase the maximum Q value), and 7.0±1.05 Å (±FWHM) neutron wavelength. The incident neutron beam was defined by two 0.8 cm inner diameter cadmium apertures that sandwiched the sample in the gas cell. All SANS data were corrected for transmission, empty beam, and dark current and placed on an absolute cross section scale using the SilA1 silica calibration standard.

3. Results and interpretation

3.1. Intermediate Q behaviour

Measurements of the hydride cycled SC(α/α′/α)14 sample, with and without deuterium, are shown in Fig. 1. This is a linear plot of the absolute differential coherent scattering cross section, $d\Sigma/d\Omega$, versus neutron wave-vector transfer, Q. The wave-vector transfer is given by $Q=(4\pi/\lambda)\sin\theta$, where θ is half the total scattering angle and λ is the neutron wavelength. A similar plot for the cold rolled SC(cw)15 sample is given in Fig. 2. One observation is immediately clear from these two figures; the effect of deuterium addition is much more pronounced for the hydride cycled sample. To facilitate a more direct comparison, the three deformed samples are shown together in Fig. 3, a ln–ln plot of the net scattering cross sections (defined as the difference between the with- and without-deuterium measurements).

The net cross sections can be modeled with a cylindrical geometry that represents the trapped deuterium at the dislocation defects. This model cross section has been developed previously and is given by the following expression [11],

$$\frac{d\Sigma}{d\Omega}(Q)=\frac{\pi b^2\rho_D^2}{\rho_d Q}\exp\left(\frac{-Q^2R_o^2}{4}\right)\left[\frac{2}{\pi}\tan^{-1}(QL_o)\right], \quad (1)$$

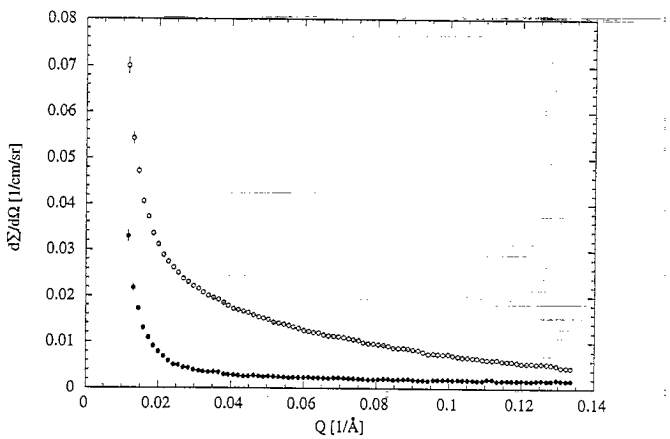

Fig. 1. Measured cross sections for hydride cycled sample SC(α/α′/α)14; with deuterium (open circles), without deuterium (closed circles).

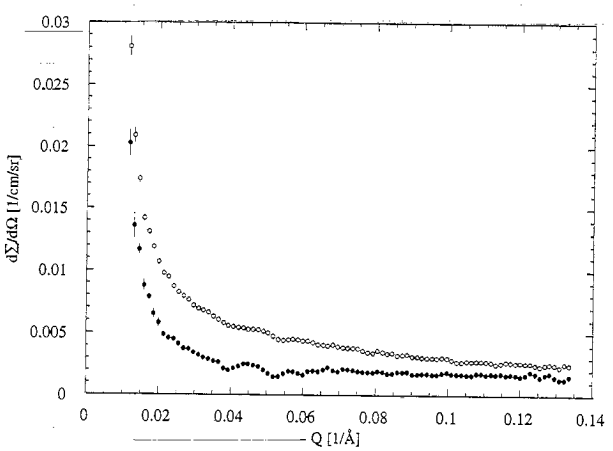

Fig. 2. Measured cross sections for cold rolled sample SC(cw)15; with deuterium (open circles), without deuterium (closed circles).

where b is the bound atom scattering length of a deuteron, ρ_D is the number density of excess deuterons trapped at dislocations, and ρ_d is the dislocation density (line length per unit volume) involved in the trapping interaction. The two geometric parameters, R_o and L_o, represent the cylinder radius and length, respectively. These parameters are corrections to the pure $1/Q$ response that would be expected from a zero-radius, infinitely long, line-like geometry. They modify the simple $1/Q$ behaviour significantly only at highest and lowest Q, respectively. The multiplicative pre-factor in Eq. (1) includes three constants. However, only the dislocation density is unknown; the excess, trapped deuteron number density is measured during deuterium loading [11] and the scattering length of a deuteron is known to be 0.667×10^{-12} cm [18].

The solid lines in Fig. 3 are best fits of Eq. (1). These fits are terminated at $Q=0.023$ Å^{-1} for the hydride cycled samples because the measured response deviates significantly from Eq. (1) at lower Q. Values of the parameters

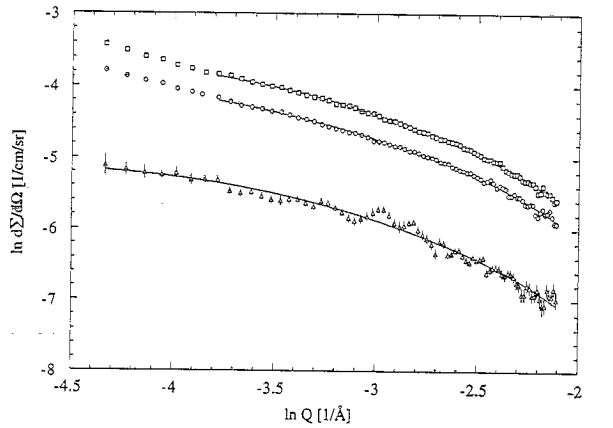

Fig. 3. Net SANS measurements (difference between with- and without-deuterium measurements) for SC(α/α′/α)12 (open circles), SC(α/α′/α)14 (open boxes), and SC(cw)15 (open triangles). Solid curves are best fits using Eq. (1). (Error bars for the cycled samples are covered by the plotting symbols.)

obtained from the best fits are given in Table 1. The measured excess deuteron densities for each sample and the number of trapped deuterons per unit length of dislocation, given by the ratio of ρ_D to ρ_d, are included in Table 1.

Reliable evidence for the R_o correction is illustrated in Fig. 4, showing plots of $\ln(Q\cdot d\Sigma/d\Omega)$ vs. Q^2 for the net data from the three deformed samples. This figure can be understood by examining Eq. (1); ignoring the inverse tangent correction term, which is justified at Q above about 0.080 1/Å, the slope of $\ln(Q\cdot d\Sigma/d\Omega)$ vs. Q^2 is equal to $-R^2/4$. The R_o values in Table 1 were obtained from best-fit slopes over the linear range above $Q\approx 0.08$ Å^{-1} in Fig. 4. The values of R_o are equal for both types of samples within experimental uncertainty and only a few Burgers vectors (2.75 Å for Pd) in magnitude. From this we conclude that most of the deuterium, including that in the non-elastic core region and the near core elastic region are characterized by a common R_o.

The R_o correction term was introduced in the model as an effective cut-off radius, within which the majority of trapped deuterons lie [11]. While this facilitated the analytical development of the model cross section, it is an over-simplification; two distributions with the same fitted R_o may have different profiles in the vicinity of R_o. The true deuterium spatial distribution about dislocations will be more gradual, especially for the cycled samples with a more uniform dislocation substructure. We then expect the intermediate Q response to include correlations beyond the 11 Å radius. This is discussed in the next section.

Tyson proposed a model in which the majority of trapped hydrogen is assumed to reside within an "extended" core about edge dislocations [12]. However, the values of R_o given in Table 1 are factor of 2.5 smaller than the extended core radius of 28 Å calculated by Tyson. We suspect this discrepancy is due to the different methods of sample preparation. Tyson applied his model to temperature-dependent, hydrogen solubility data from heavily deformed polycrystalline Pd chips (incorrectly identified as 78% cold rolled by Tyson; the Pd actually consisted of chips mechanically cut off of a disk-shaped specimen) measured by Flanagan et al. [19]. These chips showed anomalously large hydrogen enhancement ratios; for example, a ratio of 1.63 was measured at 298 K [19]. This is much larger than we obtained from our samples.

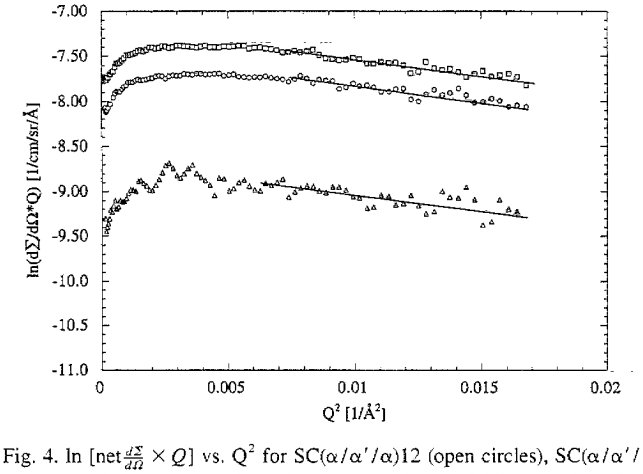

Fig. 4. ln [net$\frac{d\Sigma}{d\Omega}\times Q$] vs. Q^2 for SC(α/α′/α)12 (open circles), SC(α/α′/α)14 (open boxes), and SC(cw)15 (open triangles). Solid lines are best fits over linear, high Q portion of the data, demonstrating the effect of the R_o correction term in Eq. (1).

We have applied Tyson's extended core model to the true 78% cold rolled temperature-dependent solubility data of Flanagan et al. This sample deformation procedure is very similar to ours (except for the use of polycrystalline material) and resulted enhancement ratios consistent with those given in Table 1 [19]. The extended core model reproduces the 78% cold rolled solubility data reasonably well with an extended core radius of 11 Å (four Burgers vector units) and a dislocation density of 1.4×10^{12} cm^{-2}. The latter is approximately a factor of five larger than the densities given in Table 1. However, a direct comparison between polycrystalline and single crystal dislocation densities is not completely valid; grain boundaries induce a significant amount of hardening and the deformation of polycrystalline material will result in higher dislocation densities.

The deuterium-dislocation trapping interaction is quantified by a trapping efficiency, given as the ρ_D/ρ_d ratio (trapped deuterons per unit length of dislocation) in Table 1. It is at least a factor of two greater for the cycled samples, SC(α/α′/α)12 and SC(α/α′/α)14, than for the cold worked sample, SC(cw)15. We believe this reflects the effect of dislocation entanglement and consequent stress compensation from neighbouring dislocations in the cold worked sample. This is supported by the dislocation spacing deduced from densities in Table 1. For uniformly spaced dislocations the average separation would be roughly $1/\sqrt{\rho_d}$, which is of order 200 Å for the densities given in Table 1. This might be reached approximately for the hydride cycled samples with a uniform dislocation substructure, but cannot be expected for dislocations entangled in a cell-wall environment. One can infer that there is negligible inter-dislocation interference (that is, stress compensation) for the cycled samples out to a radius of perhaps 100 Å. On the other hand, the lower efficiency of the cold worked sample can be attributed to a reduction of near-core stress field trapping, which must extend down below 11 Å, and therefore throughout the intermediate Q range.

As expected, the with- and without-deuterium SANS measurements of the undeformed reference sample showed no net effect of deuterium trapping and are not shown. In addition, the deuterium enhancement ratio for the reference sample was 0.99±0.02; that is, no measurable defect-induced enhancement. In previous measurements of deuterium-grain boundary trapping in polycrystalline Pd, deuterium correlations with microvoids or inclusions were a suspected source of SANS interference [10]. The present

work confirms that there are no detectable correlations in the undeformed single crystal Pd material.

We note that while the cross sections shown in Fig. 3 for the hydride cycled samples have the same shape, the intensity from SC(α/α′/α)12 is down by 30% and the deduced trapping efficiency by 20%. These two samples were hydride cycled in an identical manner. However, in the course of procedural testing, SC(α/α′/α)12 underwent seven solid solution deuterium loading runs and associated pre- and post-anneals before the present experiment. (SC(cw)15 and SC(α/α′/α)14 were not loaded prior to these experiments.) We suspect the loss in performance is due to partial dislocation recovery during the annealing cycles associated with this pre-treatment history.

Comparison with results from similar samples measured on PACE at ILL, Saclay, and reported in ref. 11 are appended to Table 1. The constants for SC(α/α′/α) and SC(cw) are slightly different than those in ref. 11 because data reduction has been re-done using an improved curve fitting procedure. The larger enhancement ratios for the Saclay samples are accompanied by larger inferred ρ_d, but the efficiencies, ρ_D/ρ_d, are smaller. For the NIST data, the hydride-cycled samples show a factor of 2 to 2.5 above the cold worked sample discussed above. This systematic difference between sample deformation types is also present in the Saclay data, but to a much weaker degree.

3.2. Low Q behaviour

One important feature of Fig. 3 is the lowest Q response of the two cycled samples, SC(α/α′/α)12 and SC(α/α′/α)14. To highlight the divergence of the cycled samples from Eq. (1) and from SC(cw)15, the three net cross sections have been normalized at $Q=0.07$ Å^{-1} and re-plotted in Fig. 5. Also shown is a normalized best-fit curve from Eq. (1), now extended to the lowest Q end of the measurement. All three samples are well represented by Eq. (1) above $Q\approx0.025$ Å^{-1}. However, only SC(cw)15 follows Eq. (1) below this Q value, as was demonstrated in Fig. 3. The Q dependence of the two cycled samples are identical and rise above the model cross section at lowest Q.

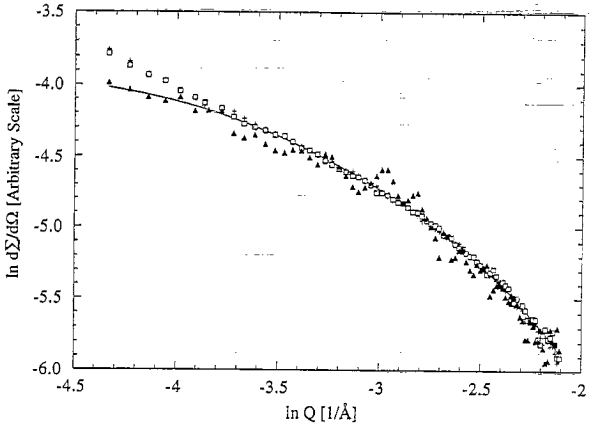

Fig. 5. Normalized net SANS measurements (difference between with- and without-deuterium measurements) for SC(α/α′/α)12 (crosses), SC(α/α′/α)14 (open boxes), and SC(cw)15 (solid triangles). Solid curve is a best fit of eqn. 1 to the normalized SC(α/α′/α)12 and SC(α/α′/α)14 data, fitted above Q=0.023 Å^{-1} only, but extended to lowest Q.

The deviation of the measured response for both the cycled samples, seen in Fig. 5, means that there is additional trapping not included in our model fitted over the intermediate Q regime. At lowest Q, the scattering is most sensitive to dimensions much larger than R_o, of order 75 Å and larger. The scattering response must contain contributions from deuterium attracted to the long range, $1/R$ stress field of dislocations in cycled material. Since this response is absent in the cold worked sample, we conclude that again this is due to the relative isolation or independence of the dislocations in the cycled material.

To quantitatively account for the additional long range trapping not characterized by the R_o cut-off radius, a model which includes a second distribution or series of additional distributions appropriate to larger dimensions is required. We do not yet feel justified to attempt such a complication, because our data do not extend adequately to lower Q. It is evident, furthermore, from Fig. 1 that scattering from deuterium-free samples becomes very large below $Q\sim0.010$ Å^{-1}, placing limitations on the resolution of deuterium-induced changes in the scattering response. Finally, the role of the L_o length correction term becomes increasingly important at lower Q. This correction represents a real physical need since the dislocations are not infinitely long and straight. For the present data, the L_o correction was definitely required to obtain good fits for all three samples over a range of $0.023<Q<0.080$ Å^{-1}.

Despite these limitations, the divergence at low Q (cold worked versus cycled samples) is in qualitative agreement with the results at intermediate Q; both observations are attributed to the more uniform dislocation substructure of the cycled material.

4. Summary

New measurements are presented from deuterium-loaded, deformed, single crystal Pd which improves and clarifies earlier results. Specifically, the SANS results confirm a difference in deuterium trapping behaviour for dislocations created by hydride cycling and cold working. The data are very well fit by a rod-like trapping geometry model for all samples above Q~0.02 Å^{-1}. In this intermediate Q regime the model fitting shows (a) that the trapping efficiency for hydride cycled samples is at least twice as great as that for cold worked samples, and (b) within experimental limit the radial "cut-off" (R_o parameter) of the trapped distribution is equal to four Burgers vectors (11 Å) for both sample types. The first result is

consistent with the assumption that the stress fields surrounding individual dislocations in cold worked material are largely neutralized by entanglement in a cell-wall environment. This compensation effect restricts both the long range ($1/R$) and short range (in the vicinity of R_0) trapping interaction. The second result appears to contradict the first. It is due, we believe, to the implementation of the exponential correction term under the condition that the majority of trapped deuterium lie within R_0 of the dislocation. This condition will be met in each sample type if trapped concentration is dominated by the core and near-core (within R_0) interaction.

The magnitude of cut-off radius is in substantial disagreement with an earlier value of 28 Å reported by Tyson using an extended core model applied to anomalously high solubility data from severely deformed Pd chips. However, an extended core radius in agreement with our R_0 value is obtained when the Tyson's model is applied to solubility data from cold rolled Pd.

At lowest Q the cold worked sample is still well described by the intermediate Q model, but the two cycled samples show an identical divergence above the rod-like geometry response. We attribute this additional scattering to a long range trapping component that extends beyond R_0 to distances of approximately 75 Å and larger. We do not yet have a model which can quantify these long range interactions for the cycled material, and additional low Q data are needed. However, the presence of a long range component is qualitatively consistent with the uniform dislocation substructure in the cycled material.

Finally we note that the measurements presented here can be viewed not only as a measure of the deuterium-dislocation trapping magnitude, but also as a probe of the local dislocation defect environment. The use of hydrogen solubility measurements as an indication of dislocation recovery has been demonstrated by Flanagan et al. [20]. In much the same way, deuterium-dislocation correlations investigated with SANS can serve as a microscopic probe of inter-dislocation stress field interactions. This is illustrated, we believe, by the lack of long range radial correlations and reduced near-core trapping efficiency of dislocations in the cell-wall environment of heavily cold rolled Pd.

Acknowledgments

This work was supported by the National Science Foundation under Grant No. DMR-9496297. It is also based upon activities supported by the National Science Foundation under Agreement No. DMR-9423101. The support of the National Institute of Standards and Technology, US Department of Commerce, in providing the facilities used in this experiment is gratefully acknowledged. The authors also greatly appreciate the assistance of Dr. John Barker of the National Institute of Standards and Technology. His assistance with the configuration and operation of NG-3 were very helpful.

Finally, we note with great sadness the death of George Summerfield on February 6, 1996. He devoted the last few years of his career to the subject of hydrogen in metals. His contributions to us are invaluable. We will miss his friendship and unique perspective on life and science.

References

[1] H. Wagner, in: G. Alefeld, J. Völkl (Eds.), Topics in Applied Physics V28: Hydrogen in Metals 1, Springer-Verlag, Berlin 1978.
[2] J.D. Clewley, T. Curran, T.B. Flanagan, W.A. Oates, J. Chem. Soc. Faraday Trans. I. 69 (1973) 449.
[3] H. Jehn, H. Speck, W. Hehn, E. Fromm, G. Hörz, Gases and Carbon in Metals, Part 19, Energie Physik Mathematik, GmbH, Karlsrule, FRG 1982.
[4] Y. de Ribaupierre, F.D. Manchester, J. Phys. C. Solid State Phys. 8 (1975) 1339.
[5] H. Frieske, E. Wicke, Ber. Bunsen-Gersellschaft. 77 (1972) 48.
[6] J. Völkl, G. Alefeld, in: A.S. Norwick, J.J. Burton (Eds.), Diffusion in Solids: Recent Advances, Academic Press, Inc., New York 1975.
[7] G. Sicking, M. Glugla, B. Huber, Ber. Bunsenges. Phys. Chem. 87 (1983) 418.
[8] R. Kirchheim, Progress in Materials Science. 32 (1988) 262.
[9] J.F. Lynch, J.D. Clewley, T. Curran, T.B. Flanagan, J. Less-Common Metals 55 (1977) 153.
[10] B.J. Heuser, J.S. King, G.C Summerfield, Defect-Interface Interactions, Mat. Res. Soc. Symp. Proc. 319 (1994) 339.
[11] B.J. Heuser, J.S. King, G.C. Summerfield, F. Boue, J.E. Epperson, Acta metall. mater. 39 (1991) 2815.
[12] W.R. Tyson, J. Less-Common Metals. 70 (1980) 209.
[13] E. Wicke, H. Brodowsky, Topics in Applied Physics V28: Hydrogen in Metals 2, Springer-Verlag, Berlin, 1978.
[14] B.J. Heuser, Ph.D. Thesis, University of Michigan, Ann Arbor, 1990.
[15] H.C. Jamieson, G.C. Weatherly, F.D. Manchester, J. Less-Common Metals. 50 (1976) 85.
[16] M.L.H. Wise, J.P.G. Farr, I.R. Harris, J.R. Hirst, L Hydrogene Dans les Metaux, Tome 1, Editions Sciences et Industrie, Paris, 1972.
[17] B. Hammouda, S. Krueger, C.J. Glinka, J. Res. NIST 98 (1993) 31.
[18] V.F. Sears, Neutron News. 3 (1992) 26.
[19] T.B. Flanagan, J.F. Lynch, J.D. Clewley, B. von Turkovich, J. Less-Common Metals 49 (1976) 13.
[20] T.B. Flanagan, J.F. Lynch, J.D. Clewley, Scripta metall. 9 (1975) 1063.